Design of AlN-Based PMUT with High Electromechanical Coupling Efficiency for Breast Cancer Diagnosis

Chang Liu[1], Yijun Cheng[1,*], Chenyang Xue[2]

[1]Department of Electronic and Engineering, Taiyuan Institute of Technology, Shanxi, China

[2]Key Laboratory of Instrumentation Science & Dynamic Measurement, North University of China, Shanxi, China

Received 18 July 2024; received in revised form 22 September 2024; accepted 24 September 2024

DOI: https://doi.org/10.46604/ijeti.2024.14017

Abstract

The study aims to develop a piezoelectric micromachined ultrasonic transducer (PMUT) with high transmission capability to achieve greater detection depth. The structural design of the sensing cell based on aluminum nitride (AlN) thin film is provided, and a mathematical theoretical model is derived. Static pressure, static displacement, vibration modes, resonant frequency, sensitivity, and acoustic impedance are analyzed using the finite element analysis. The areas of the upper and lower electrodes and the thicknesses of the piezoelectric and vibrating films are optimized. Simulation results indicate that when the ratio of the upper and lower electrodes of the sensing cells is 0.7, the electromechanical coupling efficiency of the transducer is enhanced, and its transmission performance is further improved. Mainly the first-order resonant frequency of PMUT is 7.62 MHz, with a sensitivity of −198 dB and an effective electromechanical coupling coefficient of 10.2%, meeting the design requirements for breast cancer detection.

Keywords: PMUT, AlN, electromechanical coupling efficiency, breast cancer

1. Introduction

According to statistics from the World Health Organization Cancer Research Center, the prevalence rate of female breast cancer is 30.1%, the incidence rate is 24.2%, and the mortality rate is 15% [1]. Therefore, early and accurate diagnosis is crucial to improving the survival rate of breast cancer patients. With the rapid development of ultrasonic computerized tomography (CT) technology, it is expected to become the most promising imaging method for breast cancer diagnosis [2]. Currently, research teams, both domestically and internationally, are dedicated to developing ultrasonic CT systems for early breast cancer screening. Despite significant progress, many technical challenges remain, with the traditional piezoelectric ceramic ultrasonic transducer being one of the primary obstacles [3]. This component is often cited as the most significant barrier to further innovation [4]. Even though there have been impressive advancements in electromechanical coupling, producing sensors based on advanced materials still relies on challenging manufacturing processes [5].

These processes limit component miniaturization and adversely affect image resolution, probe size, and production costs. The realization of the next generation of medical ultrasound systems requires manufacturing many inexpensive, efficient, and sensitive sensors. As an alternative, microelectromechanical systems (MEMS)-based designs show promise in the cost-effective manufacturing of large numbers of miniaturized components with improved performance using innovative sensing mechanisms [6]. Capacitive micromachined ultrasonic transducers (CMUTs) and piezoelectric micromachined

* Corresponding author. E-mail address: alexcheng@163.com

English language proofreader: Chih-Wen Teng

ultrasonic transducers (PMUTs) are the main types of ultrasonic transducers [7]. These two ultrasonic transducers have similar working principles, and both work in flexural vibration mode. It can achieve good impedance matching in the acoustic field. Compared to PMUTs, CMUTs have disadvantages in gap height, DC bias voltage, and output pressure capacity [8]. PMUTs, with their piezoelectric driving mechanism, have fewer constraints on structural design. Additionally, PMUT does not require a DC bias voltage and can achieve a high output sound pressure at a low voltage drive [6, 9].

In 1979, Shiosaki et al. [10] developed the first ultrasonic sensor based on zinc oxide (ZnO) films. In 1997, Bernstein et al. [11] invented a PMUT array based on lead zirconate titanate (PZT) films for ultrasonic imaging in water. In 2004, Yamashita et al. [12] first demonstrated three-dimensional (3D) imaging of target objects in air using thin film PZT PMUTs. In 2006, Chao et al. [13] developed a deposition method for preparing thin film polyvinylidene fluoride (PVDF), which can be used to fabricate flexible PMUT. In 2009, Shelton et al. [14] first proposed using aluminum nitride (AlN) films as the active layer of PMUT, thereby creating complementary metal oxide semiconductor (CMOS) compatible PMUT arrays. In 2012, Sammoura and Kim [15] attempted to construct an equivalent circuit model for PMUT with bimorph.

In 2015, Lu et al. [16] demonstrated a fingerprint sensor system chip, one of the most critical applications related to consumer electronics. In 2021, Jeong et al. [17] developed a manufacturing process for the flexible film PMUT, which is relevant for wearable medical applications. As a result, PMUTs have been widely used in gesture recognition, target detection, fingerprint scanning, and medical treatment [18]. In particular, it has shown great potential in diagnosing minor soft tissue lesions of the breast. Due to their high sound power and higher energy density than other MEMS conversion mechanisms, PMUTs are a promising alternative for high-resolution imaging at greater depths [19-20].

Despite promising prospects, previously studied PMUTs for medical ultrasound imaging applications are still in their infancy, and many problems need to be solved, mainly including:

(i) Low emission sound pressure leads to insufficient detection depth and low signal contrast.
(ii) Narrow bandwidth leads to poor imaging resolution and accuracy.

These limitations make the images produced by PMUT poor quality and cannot be used for accurate disease diagnosis, so improving PMUT performance is critical [21]. The proposed design in this work is characterized by a bimorph circular piezoelectric and vibrating layer with a vacuum cavity. AlN piezoelectric films are used due to their lead-free environmental protection, low-temperature deposition, low dielectric constant, compatibility with the CMOS process, good acoustic matching, and other advantages.

The upper and lower molybdenum (Mo) electrodes of the AlN piezoelectric layer give the device a higher quality factor and lower material loss. These considerations can achieve high electromechanical coupling efficiency, which in turn produces better emission performance so that there is sufficient sound pressure output to extract complex acoustic characteristic parameters inside the soft tissue to obtain high-resolution breast imaging. Due to the limited number of existing analysis models, the relationship between PMUT performance parameters and structural design parameters is still poorly understood, and further in-depth research is needed [22]. A more structured design process can be implemented by developing better predictive models that focus on a fundamental understanding of key performance indicators. This approach will enable substantial performance improvements and bring PMUT technology closer to commercial implementation.

2. Structural Design of Circular Bimorph PMUT

Given the particularity of breast soft tissue, a breast ultrasound CT system based on the cylindrical motion of the PMUT linear array was developed, as illustrated in Fig. 1. The most important feature of this system is its ability to obtain 3D tissue signals using a two-dimensional (2D) structure. Four vertically crossed PMUT linear array configurations capture both

reflected and transmitted ultrasound signals from breast tissue. The length of the array is parallel to the circular axis and roughly parallel to the central axis of the breast. The size of the linear array transducer meets the different sizes requirements for breast detection, and the maximum detection aperture is 18 cm × 13 cm. The transducer surrounds the breast tissue for cylindrical and non-contact measurement.

The whole test is carried out in the water tank (32 ℃), controlled by a computer workstation with a high-precision electric rotating table, combined with a mechanical alignment device (acrylic fixture) to drive the PMUT array to perform column scanning with a rotating accuracy of 0.05 ℃. The multi-channel ultrasonic signal transmitting/collecting circuit system drives the PMUT array to realize ultrasonic transmission and receiving control. Furthermore, characteristic parameters such as sound velocity, sound attenuation, and acoustic impedance were extracted from the ultrasonic signals. High-resolution image reconstruction was achieved using a multi-parameter fusion imaging algorithm. The performance of the PMUT, as a critical detection part of the breast ultrasound CT system, directly impacts the high specificity required for early screening and accurate diagnosis of small lesions [2].

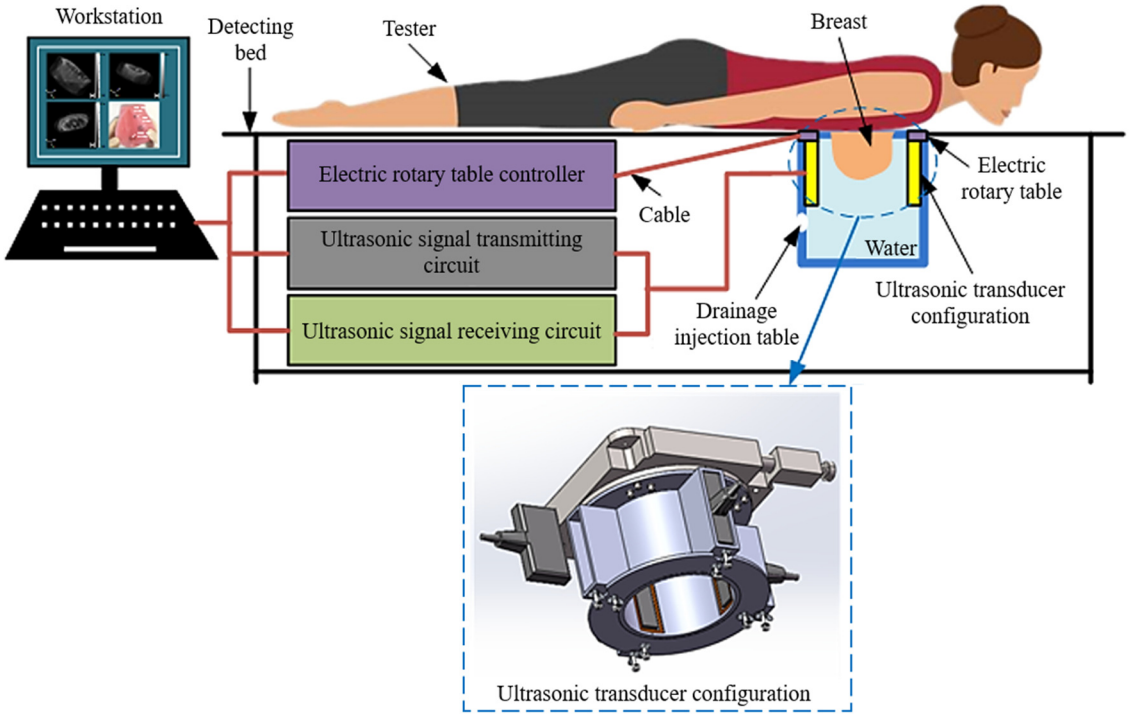

Fig. 1 Schematic diagram of breast ultrasound CT system

The circular bimorph PMUT sensing cell structure discussed in this study is illustrated in Fig. 2. The device comprises two central films: the vibrating sensing film and the supporting substrate film. The upper vibrating sensing layer primarily facilitates acoustoelectric conversion, consisting of the upper electrode Mo, the piezoelectric film AlN, the lower electrode Mo, and the vibrating film silicon (Si). The supporting substrate layer beneath serves a supportive and stabilizing role, composed mainly of the insulating layer silicon dioxide (SiO_2) and the support layer Si. AlN piezoelectric films are chosen for their low dielectric constant, excellent acoustic matching, and compatibility with CMOS technology, enhancing the PMUT design's potential for medical applications. Metal electrodes are positioned on both surfaces of the piezoelectric films. Mo, selected for its lower resistivity and higher acoustic impedance than AlN, ensures the device achieves a higher quality factor and lower material loss with consistent structural design [23].

Also, Al, chosen for its cost-effectiveness and superior electrical conductivity, is the extraction electrode for testing purposes [24]. The selection of thin film materials is crucial in PMUT design, impacting device performance and manufacturing. Material properties and dimensions significantly influence the acoustic characteristics of the film. PMUTs detect ultrasound signals within soft breast tissue during reception mode operation. In this mode, incoming pressure causes the

piezoelectric sensing film to deflect, generating transverse stress and an electrical charge across the piezoelectric layer via the piezoelectric effect. When subjected to incoming sound waves, the sensing cell's film bends up and down. This movement induces tensile stress on the outer side and compressive stress on the inner side, and vice versa. The piezoelectric films generate positive and negative charges on their surfaces due to the direct piezoelectric effect. To enhance the receiving sensitivity of the sensor, the top electrode should ideally cover areas with no changes in stress or charge.

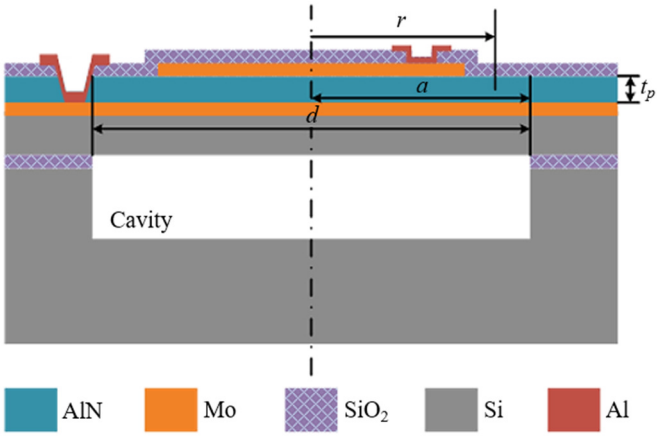

Fig. 2 PMUT sensing cell structure

The data in Table 1 is key structural parameters used in PMUT sensing cells. The transducer structure layer is composed of a 1.0 μm thick AlN piezoelectric layer, a 5.0 μm thick Si vibrating layer, and a 0.2 μm thick Mo layer as electrode from upper to lower.

Table 1 Structural parameters used in the PMUT simulation model

Parameter	Material	Radius (μm)	Thickness (μm)
Upper electrode	Mo	42	0.2
Piezoelectric film	AlN	60	1.0
Lower electrode	Mo	60	0.2
Vibrating film	Si	60	5.0

In the simulation, based on the materials of different structural layers, Table 2 shows the properties of the materials adopted in PMUT [25]. The corresponding elastic constants, relative permittivity, density, and piezoelectric stress constants are summarized from the literature as an overview. For medical imaging applications, choosing the right combination of materials is critical, which not only affects the performance of the device but may also affect its manufacturing cost and feasibility.

Table 2 Properties of the materials adopted in PMUT

		AlN	Si	SiO_2	Mo
Elastic constants, c_{ij} (GPa)	c_{11}	410.1	165.6	70	329
	c_{12}	100.7	63.9		
	c_{13}	83.8			
	c_{33}	386.2			
	c_{44}	100.6	79.5		
	c_{66}	154.7			
Relative permittivity, ε_{ij}	ε_{31}	9		4.2	
	ε_{33}	11		4.2	
Density, ρ (kg/m^3)	ρ	3260	2329	2200	10200
Piezoelectric stress constants, e_{ij} (C/m^2)	e_{ij}	–0.48			
		–0.58			
		1.55			

3. PMUT Model Analysis

The boundary condition of the piezoelectric film is regarded as a simple boundary. That is, the boundary can be bent but not moved. The deflection w at the boundary is zero, the bending moment M_r is zero, and the mathematical expression is as follows [26]:

$$\begin{cases} w\big|_{r=a} = 0, \\ M_r\big|_{r=a} = 0 \end{cases} \tag{1}$$

For the simplified model, under uniform pressure p, the deflection on the circular film at r from the center of the circle is:

$$w(r) = \frac{p}{64D_e}\left(a^2 - r^2\right)^2 \tag{2}$$

where a is the radius of the film, r is the distance from the point on the film to the center of the circle, and D_e is the equivalent bending stiffness of the film.

In normalized polar coordinates, the strain values in the radial and tangential direction can be respectively expressed as:

$$\varepsilon_r(r) = z_p \times \frac{d^2 w(r)}{dr^2} \tag{3}$$

$$\varepsilon_\theta(r) = \frac{z_p}{r} \times \frac{dw(r)}{dr} \tag{4}$$

where z_p denotes the distance to the neutral axis.

The corresponding radial and tangential stresses of the piezoelectric layer can be expressed as:

$$\sigma_r(r) = \frac{E_e}{\upsilon_e^{\,2} - 1}\left(\varepsilon_r(r) + \upsilon_e \varepsilon_\theta(r)\right) \tag{5}$$

$$\sigma_\theta(r) = \frac{E_e}{\upsilon_e^{\,2} - 1}\left(\varepsilon_\theta(r) + \upsilon_e \varepsilon_r(r)\right) \tag{6}$$

Further, the following equations were given by substituting Eqs. (3)-(4) into Eqs. (5)-(6):

$$\sigma_r(r) = \frac{E_e z_p}{\upsilon_e^{\,2} - 1}\left(\frac{\partial^2 w(r)}{\partial r^2} + \upsilon_e \times \frac{1}{r} \times \frac{\partial w(r)}{\partial r}\right) \tag{7}$$

$$\sigma_\theta(r) = \frac{E_e z_p}{\upsilon_e^{\,2} - 1}\left(\upsilon_e \times \frac{\partial^2 w(r)}{\partial r^2} + \frac{1}{r} \times \frac{\partial w(r)}{\partial r}\right) \tag{8}$$

where υ_e and E_e are equivalent to Poisson's ratio and Young's modulus of the film, and z_p is the distance between the center of the piezoelectric film and the center deflection axis.

By substituting Eq. (2) into Eqs. (7)-(8), the following relation is further obtained [26]:

$$\sigma_r(r) = \frac{E_e p z_p}{16D_e\left(1 - \upsilon_e^{\,2}\right)}\left[\left(1 + \upsilon_e\right)a^2 - \left(3 + \upsilon_e\right)r^2\right] \tag{9}$$

$$\sigma_\theta(r) = \frac{E_e p z_p}{16D_e\left(1 - \upsilon_e^{\,2}\right)}\left[\left(1 + \upsilon_e\right)a^2 - \left(1 + 3\upsilon_e\right)r^2\right] \tag{10}$$

In the assumed ideal state, the piezoelectric effect is entirely derived from the deflection caused by pressure p at a point. Accordingly, all the charge is converted, then the stress value at the point is zero. In this case, the radial stress $\sigma_r(r)$ and the tangential stress $\sigma_\theta(r)$ should satisfy the sum value of zero. Through calculation, it can be found that when r is approximately $0.7a$, the theoretical value of the total stress (sum of $\sigma_r(r)$ and $\sigma_\theta(r)$) is zero, so it should be designed here for the edge of the upper electrode [6].

The process of the piezoelectric effect and inverse piezoelectric effect is entirely reciprocal. Therefore, when the ratio of upper electrode radius to lower electrode radius is 0.7, regardless of whether PMUT works in the transmitting state or the receiving state, the electromechanical conversion efficiency is the highest, and the performance is the best. The receiving sensitivity S of PMUT can be obtained by calculating the following formula:

$$S = \frac{d_{31} t_p}{A_e \varepsilon p} \iint_{A_e} (\sigma_r + \sigma_\theta) d_s \tag{11}$$

where A_e is the area of the upper electrode, d_{31} is the piezoelectric constant, t_p is the piezoelectric layer thickness and ε is the dielectric constant of the piezoelectric film. When $r = 0.7a$, the receiving sensitivity S can be modified to [27]:

$$S = \frac{\pi a^2 E z_p d_{31} t_p}{16 \varepsilon D (1 - \upsilon)} \tag{12}$$

when the working medium is air, the resonant frequency of PMUT can be obtained by calculating the following formula [23]:

$$f_{air} = \frac{\lambda_{01} \times t}{2\pi \times d^2} \sqrt{\frac{E_{eq}}{12 \times \rho_{eq} \times \left(1 - \upsilon_{eq}^{\ 2}\right)}} \tag{13}$$

where the characteristic dimensions t is the circular film and d is the circular film diameter, E_{eq} is the elastic modulus, ρ_{eq} is the density, and υ_{eq} is Poisson's ratio. It is worth noting that these three variables are equivalent values for the multilayer film. λ_{01} = 40.8 is the correction factor of the circular film. However, When the working medium is water, the resonant frequency of PMUT can be modified to:

$$f_{water} = \frac{f_{air}}{\sqrt{1 + \frac{0.67 d \rho_{water}}{\rho_{eq}}}} \tag{14}$$

where ρ_{water} is the density of water.

4. Results

For the problem of breast cancer diagnosis, the finite element simulation software COMSOL was adopted to analyze the performance index of the designed PMUT [23]. The analysis began by recognizing that the lower fixed support layer minimizes film movement [28]. Therefore, its support effect was simulated by applying fixed constraint conditions on the boundary. Additionally, since the adhesive layer does not contribute to the electromechanical behavior of the film, COMSOL assumes a perfect bond between layers by default, allowing us to ignore the thickness of the bonding layer. Furthermore, the PMUT device features a symmetrical structure with the film thickness direction as the central axis. This symmetry allows the entire model to be realized by rotating a half section when establishing the simulation model. This approach significantly simplifies the calculation, ensures the accuracy of the device simulation, reduces simulation time, and improves the operation efficiency of the simulation. The methodological steps of COMSOL simulation are shown in the Fig. 3.

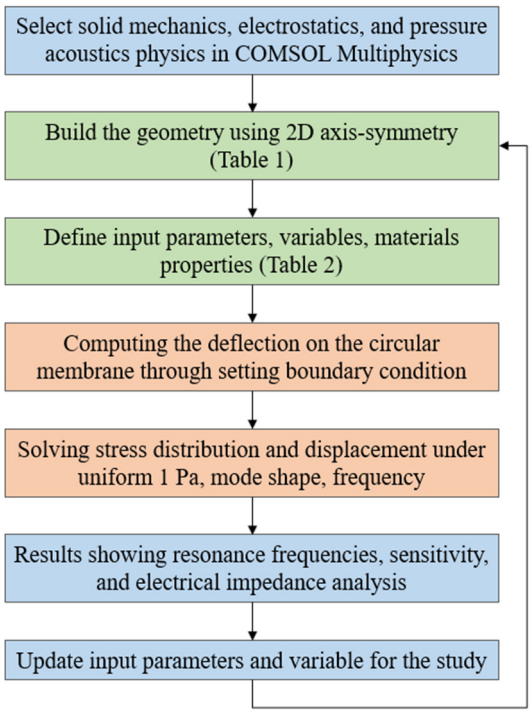

Fig. 3 The methodological steps of COMSOL simulation

Various tissues of the human body have very different absorption coefficients of ultrasound, and generally, the attenuation coefficient of soft tissues ranges from 0.6 to 0.7 dB/cm/MHz [29]. Therefore, if a higher transmission frequency is used, such as 5 MHz to 40 MHz, the wavelength of the ultrasonic wave is very small, and a higher detection resolution can be obtained, but the detection depth will be limited because the signal attenuation is too fast. When the detection depth is greater than 18 cm, the ultrasonic transmission frequency should not be less than 3.5 MHz, otherwise it is difficult to obtain the internal characteristics of the tissue.

According to the characteristics of the system, to achieve stereoscopic accurate detection of breast tissue, a detection depth of 18 cm is required to obtain relatively complete longitudinal profile data. In addition, the stereoscopic examination of the breast is performed in water. Thus, this paper intends to design an ultrasonic transducer with an operating frequency of 3.5 MHz to obtain a high detection resolution as far as possible under the premise of satisfying the detection depth. According to the calculation of Eq. (14), the frequency of ultrasonic signals in water is about 0.44 times that in air. Hence, when the designed ultrasonic transducer uses air as the medium, its resonant frequency needs to reach about 7.5 MHz.

4.1. Static pressure and displacement analysis

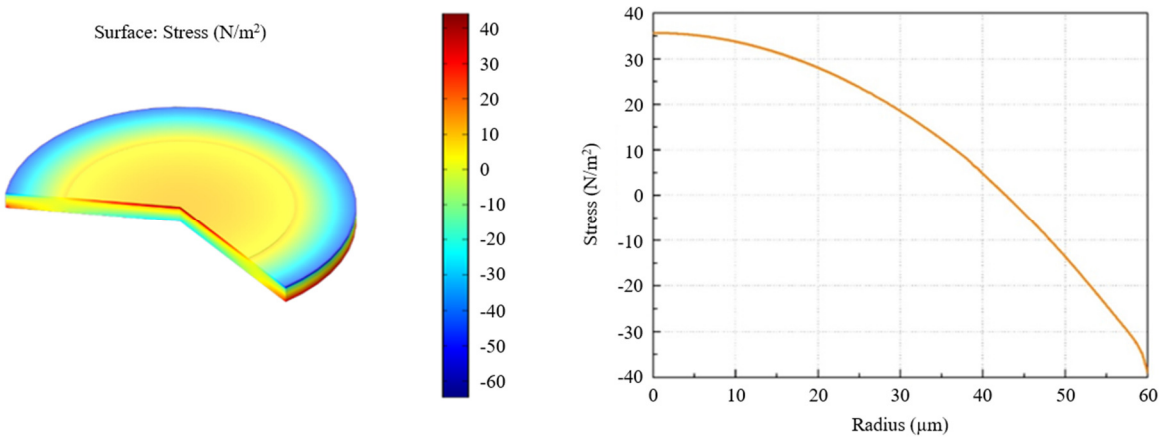

(a) Film pressure distribution

Fig. 4 Film pressure and displacement distribution at a uniform sound pressure of 1 Pa

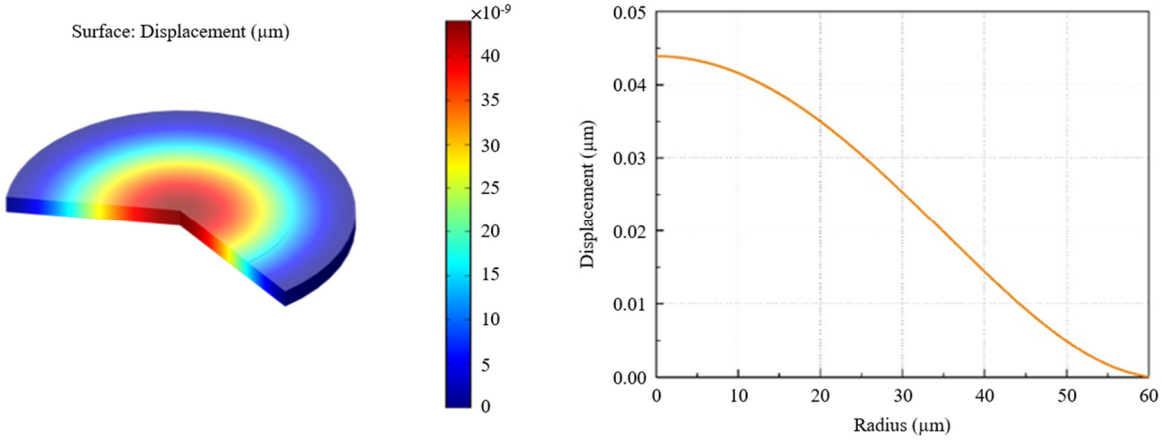

(b) Film displacement distribution

Fig. 4 Film pressure and displacement distribution at a uniform sound pressure of 1 Pa (continued)

When a uniform sound pressure of 1 Pa is exerted on the PMUT device, the stress and displacement distribution of the film are depicted in Fig. 4. The stress of the piezoelectric film is transferred from the center to the edge. The compressive stress of the center is positive, and the tensile stress of the edge is negative. Specifically, the stress value at the center is 35.68 N/m^2, while the pressure value at the edge is -39.05 N/m^2, as illustrated in Fig. 4(a). Static displacement attains a maximum of 0.044 μm at the center, gradually decreasing to 0 μm at the edge, as illustrated in Fig. 4(b). This behavior aligns with the theoretical values calculated using Eq. (2).

4.2. Modal analysis

Additionally, the modal shapes of the proposed sensing cell structure were simulated by the finite element analysis (FEA). Modal analysis helps determine a structure's vibration mode and natural frequency based on its design and material properties. Under the boundary condition where one end is free, and the other is fixed, the first six resonant modes of the device were obtained, as shown in Fig. 5.

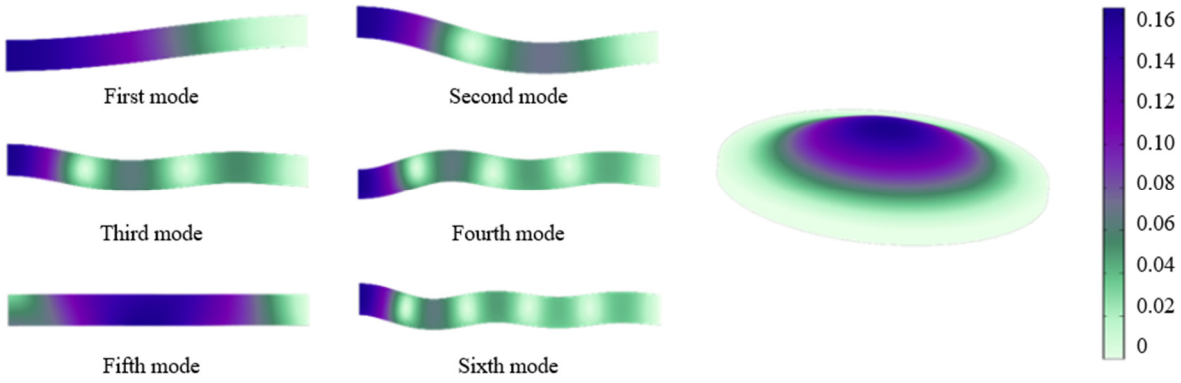

Fig. 5 The first six resonant modes

The corresponding natural frequencies are 7.61 MHz, 27.69 MHz, 56.65 MHz, 91.07 MHz, 93.44 MHz, and 128.99 MHz, respectively. As the mode order increases, more stagnation points appear in the middle of the thin plate. This results in a decrease in longitudinal resonance displacement and, consequently, a reduction in energy conversion efficiency. Therefore, the vibration is axisymmetric at the first mode or fundamental frequency and has the largest amplitude. Therefore, the fundamental mode drive is ideal for ultrasonic transduction applications. For circular thin plates, the deflection profile is related to a constant specific to each mode, which is numerically determined by the boundary conditions. This mode constant is a part of the deflection equation and directly influences the resonant frequency. Generally, the desired vibration mode during the design phase is the first mode. In this context, Eq. (9) specifies the constant as λ_{01}, where 01 denotes the first-order mode.

4.3. Resonance frequency analysis

The device operates in the first-order mode, and a harmonic response analysis was conducted. According to the calculation of the natural frequency of the first mode, the simulation frequency range was set from 6 MHz to 9 MHz, with a scanning interval of 1 kHz. Fig. 6 illustrates that the vibration displacement of the device is obtained at the central node of the circular thin plate. The calculated resonant frequency was 7.61 MHz. At this frequency, the device's amplitude peaks, with a maximum displacement of 34.2 μm. The deformation of the film is primarily determined by its bending stiffness. The device model's prediction is refined using the finite element model, which offers a detailed understanding of the physical principles controlling this deformation. This understanding can effectively guide the film's and the cavity's design.

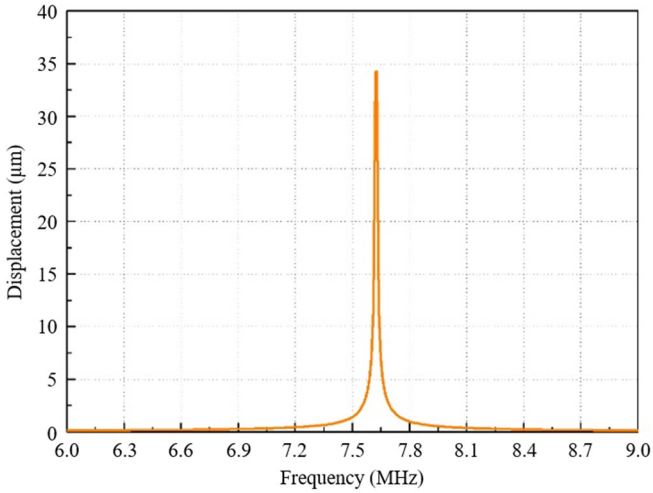

Fig. 6 Resonance frequency analysis

4.4. Sensitivity analysis

PMUT free field voltage receiving sensitivity M_e is the decibel form of the ratio V_{oc} output by the transducer to P at the location of the transducer, that is:

$$M_e = 20\lg\frac{V_{oc}}{P} - 120 \tag{15}$$

where V_{oc} is the open circuit voltage, and P is the free pressure.

Me is obtained by simulation, while S is the theoretical value calculated from the designed structural parameters. The device's sensitivity can be obtained by using Eq. (15) in COMSOL and the receiving sensitivity M_e is −198 dB (re: 1 V/μPa) over a bandwidth of 6 MHz to 9 MHz, which agrees well with the sensitivity S predicted from Eq. (12), as shown in Fig. 7.

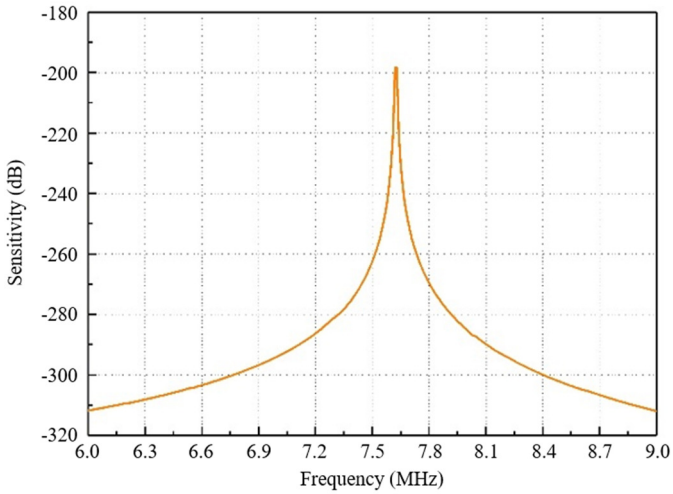

Fig. 7 Sensitivity analysis

The half-power point frequency f_1 before the resonant point is 7.60 MHz, and the half-power point frequency f_2 after the resonant point is 7.62MHz, and the quality factor Q_m calculated according to the formula below is 380.5. The value of Q will affect the mode shape and frequency selectivity of the film when the PMUT cell resonates, and thus determine the emission sensitivity of the PMUT array.

$$Q_m = \frac{f_r}{f_2 - f_1} \tag{16}$$

where f_1 and f_2 are half-power points, and Q_m is the mechanical quality factor.

4.5. Impedance analysis

Because it is the most consistently defined, the electromechanical coupling coefficient can be used to compare various PMUT designs. The impedance-frequency response curve of the device is depicted in Fig. 8. The resonant frequency f_r is 7.61 MHz, the anti-resonant frequency f_a is 7.65 MHz, and the effective electromechanical coupling coefficient K_{eff}, calculated using the following formula, is 10.2%.

$$K_{eff}^{\ 2} = 1 - \left(\frac{f_r}{f_a}\right)^2 \tag{17}$$

where f_r is the resonant frequency, and f_a is the anti-resonant frequency.

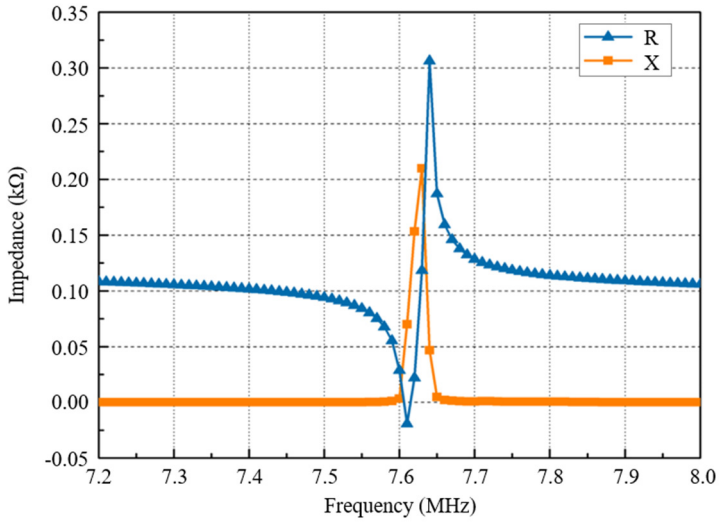

Fig. 8 Impedance-frequency response curve

Fig. 9 depicts the modulus curve of the impedance. It shows that the minimum impedance value at resonance is 35 Ω, while the maximum impedance value at anti-resonance reaches 310 Ω. The finite element model is utilized to ascertain the maximum achievable electromechanical coupling coefficient, providing crucial insights for optimizing the device design. Additionally, impedance analysis is employed for impedance matching design, guiding the optimal configuration of the device to achieve peak performance. This approach ensures that the device operates efficiently and effectively in its intended application.

The accurate diagnosis of breast cancer relies on high-resolution imaging. In traditional B-ultrasound detection, a reflection signal (acoustic impedance) is mainly used, which is conducive to obtaining tissue edge information, but difficult to detect tissue internal characteristics. The high electromechanical coupling efficiency can ensure that there is enough transmission performance to obtain tissue transmission signals (sound velocity, sound attenuation), combined with multi-parameter fusion imaging technology, to achieve high-contrast imaging of adipose glandular, cancers, fibroadenoma, cysts, calcifications, and other small lesions.

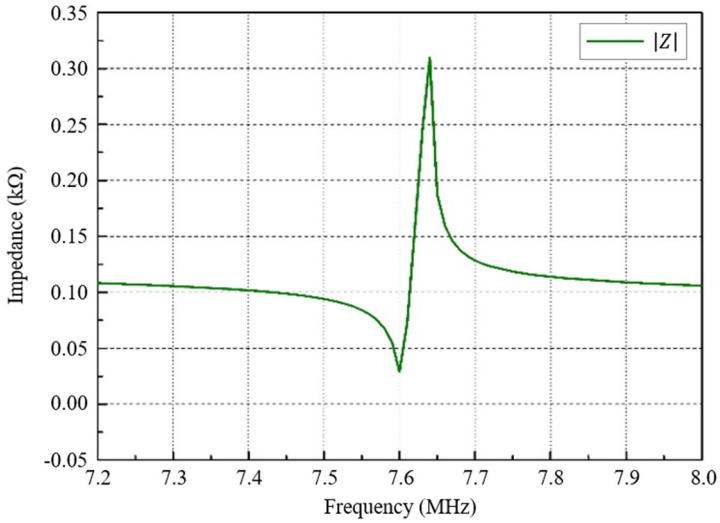

Fig. 9 Modulus curve of impedance

4.6. *Fabrication techniques for PMUT*

The predominantly used techniques to fabricate PMUTs are discussed here, as shown in Fig. 10. This project proposes to use AlN film as the piezoelectric layer, and the device is fabricated on a double-sided polished silicon-on-insulator (SOI) wafer with a vacuum cavity. The sputtering system is used to deposit Mo/AlN/Mo layers on the SOI substrate. In a subsequent etching step, Mo/AlN/Mo microdisks are formed using a patterned SiO_2 layer as a mask by combining reactive ion etching (RIE) with chlorine (Cl_2) and boron trichloride (BCl_3) gases and using helium (He) to carry away the waste. Then, 0.2 µm holes are etched in the SiO_2 insulation layer to connect the top and bottom electrodes to the top metal layer. Finally, a top metal layer is deposited and forms the wire and pad area.

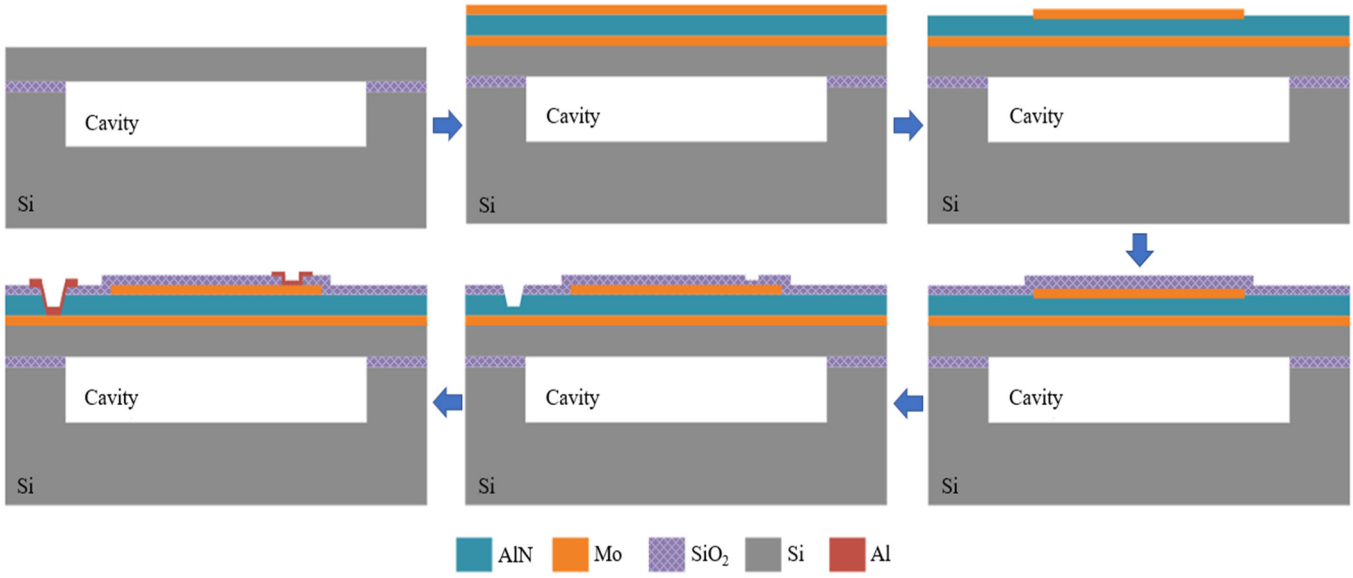

Fig. 10 Fabrication technology for PMUT

The transmitting performance of the PMUT would be characterized by directly measuring the vibrating velocities of the transduction film of the PMUT cells using the laser Doppler vibrometer (LDV). A continuous sine wave excitation signal is applied to the PMUT. The signal frequency is scanned from 6 MHz to 9 MHz. The maximum vibration displacement can be captured, which is the first-order resonance frequency of the PMUT. The acoustic pressure sensitivity of the PMUT can be measured using an industry-standard ultrasound sensor verification unit (re: 1 V/µPa). The impedance-frequency spectrum of the PMUT can be characterized by an inductor-capacitor-resistor (LCR) impedance analyzer. Important parameters can be obtained, such as resonant frequency, anti-resonant frequency, and effective electromechanical coupling coefficient.

There are still some foreseeable challenges in integrating the prepared PMUT with existing systems for clinical diagnosis. Among them, multi-mode imaging needs to collect reflected and transmitted signals, so it is necessary to solve the problem of sensor fixation and alignment. For obtaining the total volume data acquisition of breast tissue, it is necessary to perform electric rotary scanning, so the electromagnetic interference problem that occurred during the scanning process must be solved. To obtain high-resolution imaging, it is necessary to solve the problem of mutual interference between complex signals in the process of ultrasound propagation, and the problem of rapid reconstruction of breast stereoscopic detection data.

5. Conclusions

A novel design scheme for a circular bimorph PMUT based on AlN thin film was proposed and optimized using FEA. The optimized design with a top-to-bottom electrode ratio of 0.7 aimed to enhance ultrasonic transmission capability.

(1) The results of FEA indicated that the resonant frequency of the PMUT in the air was measured at 7.61 MHz, which closely aligns with the theoretical value of 7.5 MHz calculated from Eq. (13), confirming the accuracy of the FEA model. Furthermore, it is estimated that the resonant frequency in water is approximately 3.5 MHz, indirectly demonstrating suitability for breast cancer detection requirements.

(2) Sensitivity analysis is performed, in which a quality factor Q_m of 380.5 and a receiving sensitivity M_e of −198 dB are obtained. These values will affect the mode shape and frequency selectivity of the film when the PMUT cell resonates.

(3) When satisfying the center frequency of 7.5 MHz, the PMUT achieves an electromechanical coupling efficiency of 10.2%. The PMUT developed in the current work outperforms the previous high-frequency PMUT designs in electromechanical coupling coefficient, representing an advancement in high-frequency PMUT technology.

Future improvements made may include Scandium doping of the AlN piezoelectric layer, optimizing the sensing cell layout for a PMUT linear array, and extracting acoustic parameters of breast tissue for a multi-parameter fusion ultrasound algorithm. These enhancements aim to achieve high-resolution imaging for the early diagnosis of small breast lesions.

Acknowledgments

This research was funded by a fundamental research program of Shanxi province (202103021223346, 20210302124099) and a program for the discipline leaders of the Taiyuan Institute of Technology.

Conflicts of Interest

The authors declare no conflict of interest.

References

[1] B. Chen, F. Chu, X. Liu, Y. Li, J. Rong, and H. Jiang, "AlN-Based Piezoelectric Micromachined Ultrasonic Transducer for Photoacoustic Imaging," Applied Physics Letters, vol. 103, no. 3, article no. 031118, 2013.

[2] C. Liu, B. Zhang, C. Xue, W. Zhang, G. Zhang, and Y. Cheng, "Multi-Perspective Ultrasound Imaging Technology of the Breast with Cylindrical Motion of Linear Arrays," Applied Sciences, vol. 9, no. 3, article no. 419, 2019.

[3] Y. Fu, S. Sun, Z. Wang, P. Niu, M. Zhang, S. Chen, et al., "Piezoelectric Micromachined Ultrasonic Transducer with Superior Acoustic Outputs for Pulse-Echo Imaging Application," IEEE Electron Device Letters, vol. 41, no. 10, pp. 1572-1575, 2020.

[4] Y. Q. Chen, Y. X. Li, Y. Chen, Z. Y. Ju, L. Q. Tao, Y. Pang, et al., "Large-Scale and High-Density PMUT Array Based on Isolated Sol-Gel PZT Membranes for Fingerprint Imaging," Journal of The Electrochemical Society, vol. 164, no. 7, pp. B377-B381, 2017.

[5] A. Dangi and R. Pratap, "System Level Modeling and Design Maps of PMUTs with Residual Stresses," Sensors and Actuators A: Physical, vol. 262, pp. 18-28, 2017.

[6] L. Jia, L. Shi, C. Liu, C. Sun, and G. Wu, "Enhancement of Transmitting Sensitivity of Piezoelectric Micromachined Ultrasonic Transducers by Electrode Design," IEEE Transactions on Ultrasonics, Ferroelectrics, and Frequency Control, vol. 68, no. 11, pp. 3371-3377, 2021.

[7] L. Jia, L. Shi, Z. Lu, C. Sun, and G. Wu, "A High-Performance 9.5% Scandium-Doped Aluminum Nitride Piezoelectric MEMS Hydrophone with Honeycomb Structure," IEEE Electron Device Letters, vol. 42, no. 12, pp. 1845-1848, 2021.
[8] T. Xu, L. Zhao, Z. Jiang, S. Guo, Z. Li, P. Yang, et al., "Array Design of Piezoelectric Micromachined Ultrasonic Transducers with Low-Crosstalk and High-Emission Performance," IEEE Transactions on Ultrasonics, Ferroelectrics, and Frequency Control, vol. 67, no. 4, pp. 789-800, 2020.
[9] Y. Qiu, J. V. Gigliotti, M. Wallace, F. Griggio, C. E. M. Demore, S. Cochran, et al., "Piezoelectric Micromachined Ultrasound Transducer (PMUT) Arrays for Integrated Sensing, Actuation and Imaging," Sensors, vol. 15, no. 4, pp. 8020-8041, 2015.
[10] T. Shiosaki, T. Yamamoto, A. Kawabata, R. S. Muller, and R. M. White, "Fabrication and Characterization of ZnO Piezoelectric Films for Sensor Devices," International Electron Devices Meeting, pp. 151-154, 1979.
[11] J. J. Bernstein, S. L. Finberg, K. Houston, L. C. Niles, H. D. Chen, L.E. Cross, et al., "Micromachined High Frequency Ferroelectric Sonar Transducers," IEEE Transactions on Ultrasonics, Ferroelectrics, and Frequency Control, vol. 44, no. 5, pp. 960-969, 1997.
[12] K. Yamashita, L. Chansomphou, H. Murakami, and M. Okuyama, "Ultrasonic Micro Array Sensors Using Piezoelectric Thin Films and Resonant Frequency Tuning," Sensors and Actuators A: Physical, vol. 114, no. 2-3, pp. 147-153, 2004.
[13] C. Chao, T. Y. Lam, K. W. Kwok, and H. L. W. Chan, "Piezoelectric Micromachined Ultrasonic Transducers Based on P(VDF-TrFE) Copolymer Thin Films," 15th IEEE International Symposium on the Applications of Ferroelectrics, pp. 120-123, 2006.
[14] S. Shelton, M. L. Chan, H. Park, D. Horsley, B. Boser, I. Izyumin, et al., "CMOS-Compatible AlN Piezoelectric Micromachined Ultrasonic Transducers," IEEE International Ultrasonics Symposium, pp. 402-405, 2009.
[15] F. Sammoura and S. G. Kim, "Theoretical Modeling and Equivalent Electric Circuit of a Bimorph Piezoelectric Micromachined Ultrasonic Transducer," IEEE Transactions on Ultrasonics, Ferroelectrics, and Frequency Control, vol. 59, no. 5, pp. 990-998, 2012.
[16] Y. Lu, H. Tang, S. Fung, Q. Wang, J. M. Tsai, M. Daneman, et al., "Ultrasonic Fingerprint Sensor Using a Piezoelectric Micromachined Ultrasonic Transducer Array Integrated with Complementary Metal Oxide Semiconductor Electronics," Applied Physics Letters, vol. 106, no. 26, article no. 263503, 2015.
[17] Y. Jeong, J. Genoe, P. Gijsenbergh, J. Segers, P. L. Heremans, and D. Cheyns, "Fully Flexible PMUT Based on Polymer Materials and Stress Compensation by Adaptive Frequency Driving," Journal of Microelectromechanical Systems, vol. 30, no. 1, pp. 137-143, 2021.
[18] J. Zang, Z. Fan, P. Li, X. Duan, C. Wu, D. Cui, et al., "Design and Fabrication of High-Frequency Piezoelectric Micromachined Ultrasonic Transducer Based on an AlN Thin Film," Micromachines, vol. 13, no. 8, article no. 1317, 2022.
[19] T. Yang, Q. Wang, Z. Zhang, Z. Liao, Y. Zhao, Y. Li, et al., "Design and Implementation of 6 × 6 Array Piezoelectric AlN Hydrophone with High Sensitivity," IEEE Sensors Journal, vol. 21, no. 23, pp. 26615-26623, 2021.
[20] Y. Yang, H. Tian, Y. F. Wang, Y. Shu, C. J. Zhou, H. Sun, et al., "An Ultra-High Element Density pMUT Array with Low Crosstalk for 3-D Medical Imaging," Sensors, vol. 13, no. 8, pp. 9624-9634, 2013.
[21] X. Xu, Y. Gong, Z. Wang, Y. Ma, C. Yu, W. Wei, et al., " Equidimensional Piezoelectric Micromachined Ultrasonic Transducer Array with Synchronously Improved Bandwidth and Sensitivity," Journal of Microelectromechanical Systems, vol. 33, no. 5, pp. 511-513, 2024.
[22] J. Li, W. Ren, G. Fan, and C. Wang, "Design and Fabrication of Piezoelectric Micromachined Ultrasound Transducer (PMUT) with Partially-Etched ZnO Film," Sensors, vol. 17, no. 6, article no. 1381, 2017.
[23] W. Liu, L. He, X. Wang, J. Zhou, W. Xu, N. Smagin, et al., "3D FEM Analysis of High-Frequency AlN-Based PMUT Arrays on Cavity SOI," Sensors, vol. 19, no. 20, article no. 4450, 2019.
[24] W. Liu and D. Wu, "Low Temperature Adhesive Bonding-Based Fabrication of an Air-Borne Flexible Piezoelectric Micromachined Ultrasonic Transducer," Sensors, vol. 20, no. 11, article no. 3333, 2020.
[25] L. Jia, L. Shi, C. Liu, Y. Yao, C. Sun, and G. Wu, "Design and Characterization of an Aluminum Nitride-Based MEMS Hydrophone with Biologically Honeycomb Architecture," IEEE Transactions on Electron Devices, vol. 68, no. 9, pp. 4656-4663, 2021.
[26] Q. Wang, L. Zhao, T. Yang, Z. Liao, X. Xue, B. Wu, et al., "A Mathematical Model of a Piezoelectric Micro- Machined Hydrophone with Simulation and Experimental Validation," IEEE Sensors Journal, vol. 21, no. 12, pp. 13364-13372, 2021.
[27] T. Wang and C. Lee, "Zero-Bending Piezoelectric Micromachined Ultrasonic Transducer (PMUT) with Enhanced Transmitting Performance," Journal of Microelectromechanical Systems, vol. 24, no. 6, pp. 2083-2091, 2015.
[28] R. Mukhiya, R. Gopal, B. D. Pant, V. K. Khanna, and T. K. Bhattacharyya, "Design, Modeling and FEM-Based Simulations of a 1-DoF MEMS Bulk Micromachined Piezoresistive Accelerometer," Microsystem Technologies, vol. 21, no. 10, pp. 2241-2258, 2015.
[29] C. Liu, B. Zhang, C. Xue, G. Zhang, W. Zhang, and Y. Cheng, "The Application of Adaptive Time Gain Compensation in an Improved Breast Ultrasound Tomography Algorithm," Applied Sciences, vol. 9, no. 12, article no. 2574, 2019.